Final report
LIGO-T010155-00-D

Surf 2001
Rosalia Stellacci
University of Pisa

LIGO Project

Measurement of metal creep in gravitational wave detectors

Contents

Mentors

Francesco Fidecaro, Riccardo De Salvo

Chapter 1

Super Attenuator System

The seismic noise to low frequencies limits the interferometer antenna's sensivity to detect gravitational waves. The gravitational waves' spatial deformations are on the order of 10^{-21} (ratio between the spatial deformations and the distance among the mirrors of interferometer).

To achieve this sensivity is mainly about the reduction of the background noises provoked by seismic vibrations and thermal noise, which cause the mirrors to oscillate. This reduction is achieved using a Super Attenuator System, a system of pendula from which the mirrors are suspended.

In detail, a system of galley springs attenuates the seismic vertical noise .The wire that sustains following filters is suspended in the middle of this first filter. A trapezoidal steel blade constitutes each individual spring.

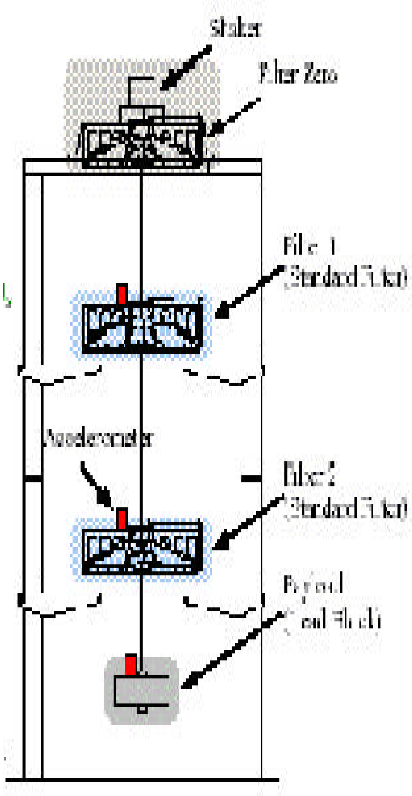

Test Tower

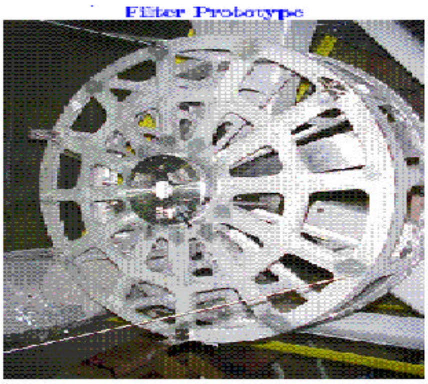

Many experiments on the super attenuator point out a metal creep phenomenon on those blades that in months or years would compromise the filter functionality. Then studies have been started about the creep phenomenon on blades, to use a right material to build this kind of filter.

Chapter
2

Creep Phenomenon

A stress applied on a metal material can provoke a progressive deformation during time. This deformation speeds up at higher temperature and it is called "metal creep".

At the beginning, there is an instantaneous deformation of the material with speed decreasing logarithmically; this stage is called "primary creep". If the material is excessively loaded there is a secondary creep, the deformation speed stabilizes to a linear behavior. This stage is the most dangerous; in fact if it is present at all the material could eventually break . Most material work in this state but with fracture times longer than our life time at higher stress, just before the material fracture there is the last stage, the tertiary stage, in witch the deformation speed increases rapidly.
By the microscopically point of view, the dislocations of the crystalline structure can explain more of the macroscopic deformation.
A crystal lattice of atoms composes the metallic material.
This lattice can have some defects called "dislocation" which change the equilibrium of atoms. We can scheme two principal kind of dislocation: " edge" (⊥) and "screw" .
To see a typical example of edge dislocation, let take a cubic crystal and let insert an atoms plane along the ABCD line. The additional atoms and grid atoms interaction changes the equilibrium position along the line CD. This line defines the edge dislocation.

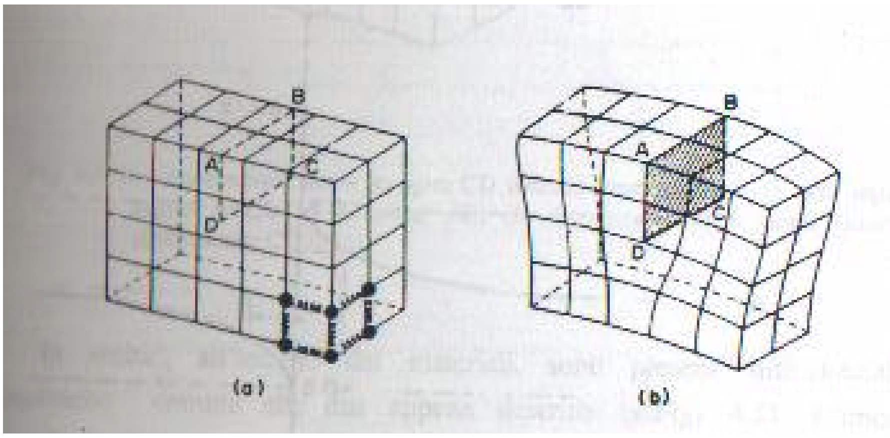

Fig.1. Edge creep

If after the sides glace, we obtain the helix configuration, as shown in the following figure, and we obtain the screw dislocation along the line CD.

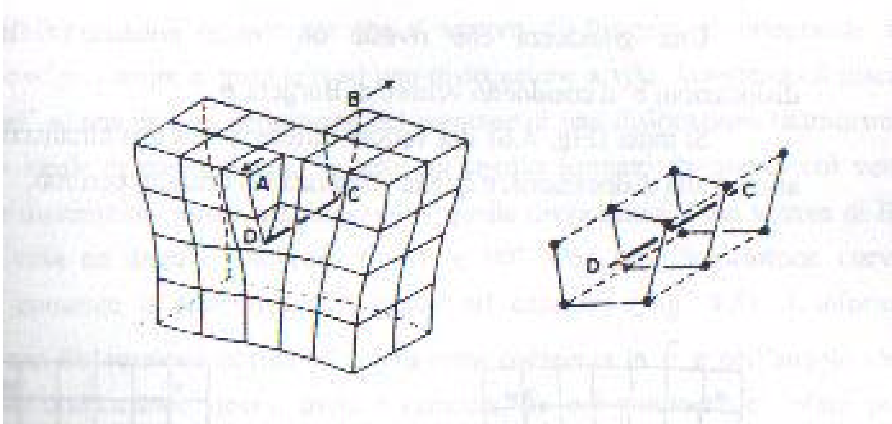

Fig.2. Screw creep

When a metal is under stress, the dislocations can propagate along the perpendicular direction to the dislocation line, without a material transport but with only dislocation propagation. The phenomenon is more evident when the material temperature increase because the rise of kinetic energy inside the lattice.

Chapter

3

Experimental Setup

The aim of the measurement is to study the behavior of specially treated maraging steel springs under high load to measure his creep rate. Having a low creep rate (~ 1 μm/day) is essential to build mechanical devices that don't introduce noise in gravitational wave detector. The measurement is done using position sensors (LVDTs) that give the position of a loaded cantilever spring. The measurement must be performed in stable temperature conditions.

Mechanics

Several blades of different thickness and length are available to be loaded on a structure called "totem". A hydraulic loading system is available to put springs under stress and to load them with steel disks bent.

The final configuration is shown in the following figure.

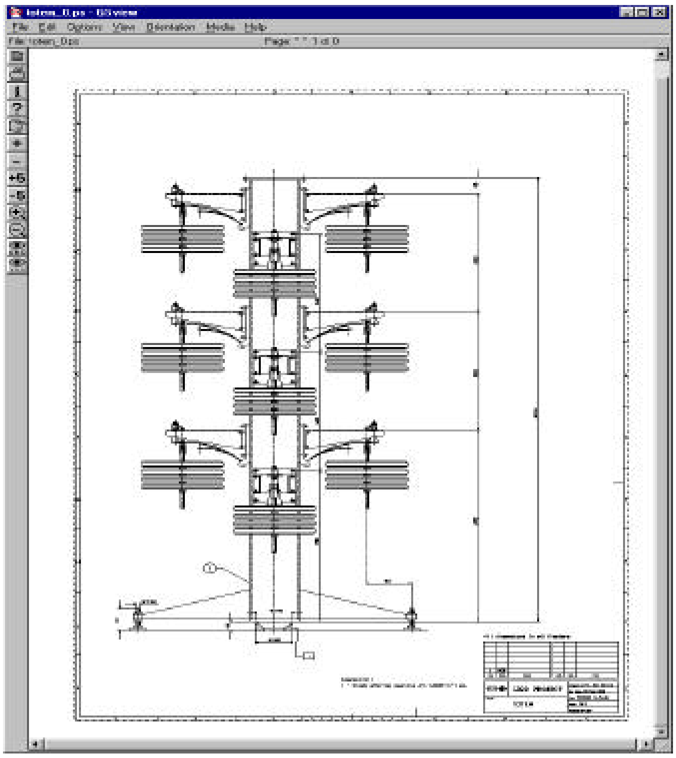

Fig. 3. Final mechanics configuration, also known as “Totem”.

A multichannel LVDT readout system was available. The block diagram is shown in fig.3. This system has been put in operation and debugged.

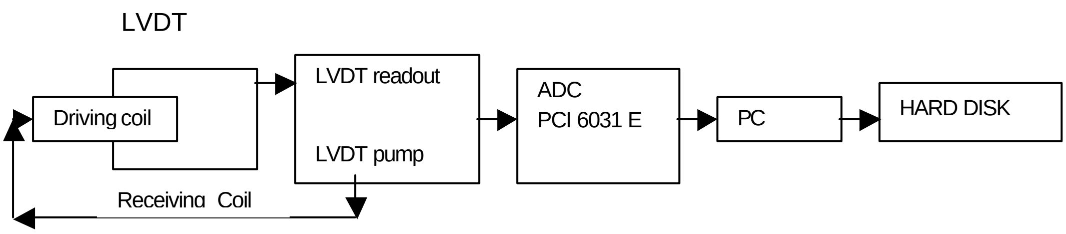

Fig. 4. Data acquisition block diagram.

The detailed electronics layout is shown in Fig. 5.

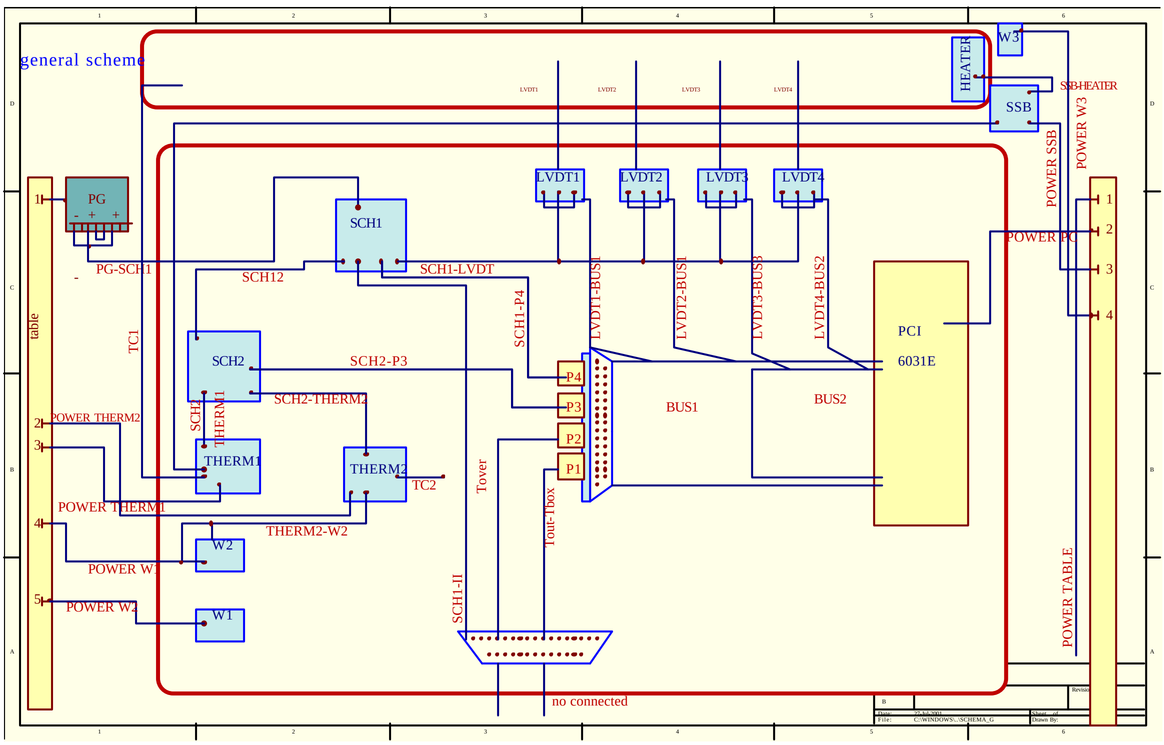

Fig. 5. Electronics layout.

As shown in figure 5, a system of two digital controllers keep the temperature inside the thermally insulted electronics box and totem box stabilized within 0.1 °C.

LVDT Sensor: two coils compose the LVDT sensor. A *pump signal*, a sinusoidal signal, is sent in the primary coil, that is the one inside the LVDT.
This driving coil current induces an electromagnetic field and a current on the secondary coil. Two separated coils wrapped up in inverted phase, compose the secondary coil.
We can measure the primary coil movement with respect to the secondary coil measuring the induced signal on the secondary coil .

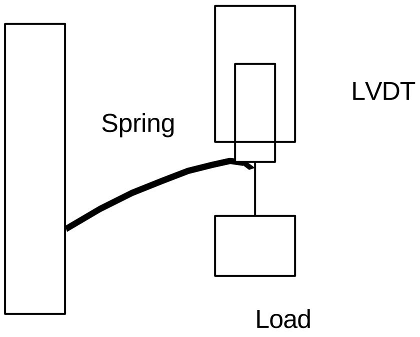

Fig.6.

LVDT Driver: This board sends a pump signal in the primary coil of the LVDT sensor and receives the potential difference from the secondary coil. It amplifies this signal, rectifies it and sends it to the acquisition board. The circuit scheme is in the following page, where RX is the signal coming from the LVDT secondary coil, TX is the pump signal sent to the primary coil and the OUT is the amplified signal output. The circuit takes a RX sinusoidal signal and compares it with the pump sinusoidal signal to demodulate the it. The demodulated amplified signal gives a potential level signal sent to acquisition board and directly proportional to the primary coil movement.

Acquisition Board: To acquire the signal coming from the LVDT drivers, we used a PCI 6031, an acquisition board equipped with 64 channels. To reduce the noise, we used the board in differential mode obtaining 32 channels.
LabView software reads the data.

Chapter 4

Software

Data Acquisition software: A Labview program has been developed, starting from a simpler version, to read the data coming from the ADC.
The programs shows in 32 graphs the LVDT readout in real time at up to 250 cycles/second and writes on a text file at fixed time interval average of LVDT readout.
From the frontal panel is possible to choose the <u>scan rate,</u> the <u>buffer size</u> and the <u>number of read out cycles</u> over witch average each data run length.

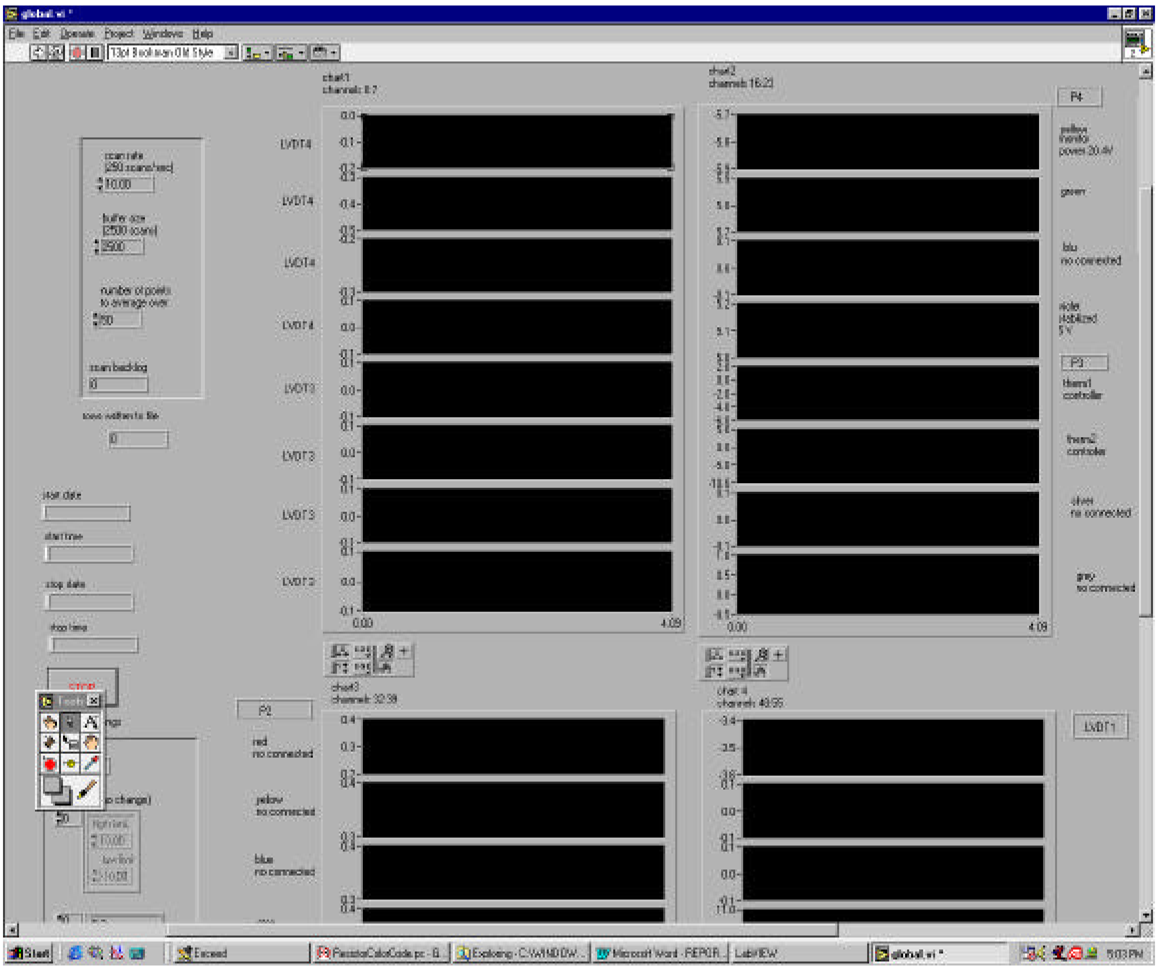

The data is FTP transferred under request from an analysis computer.

Analysis software: A MatLab program run on another PC or on a SUN workstation reads the data from the text file and draws the signals as a function of time.
Fig. 8 shows a typical set of voltages vs. time. The abscissa is in hours and the ordinate in volts.

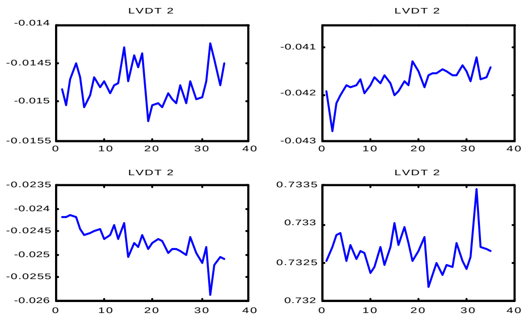

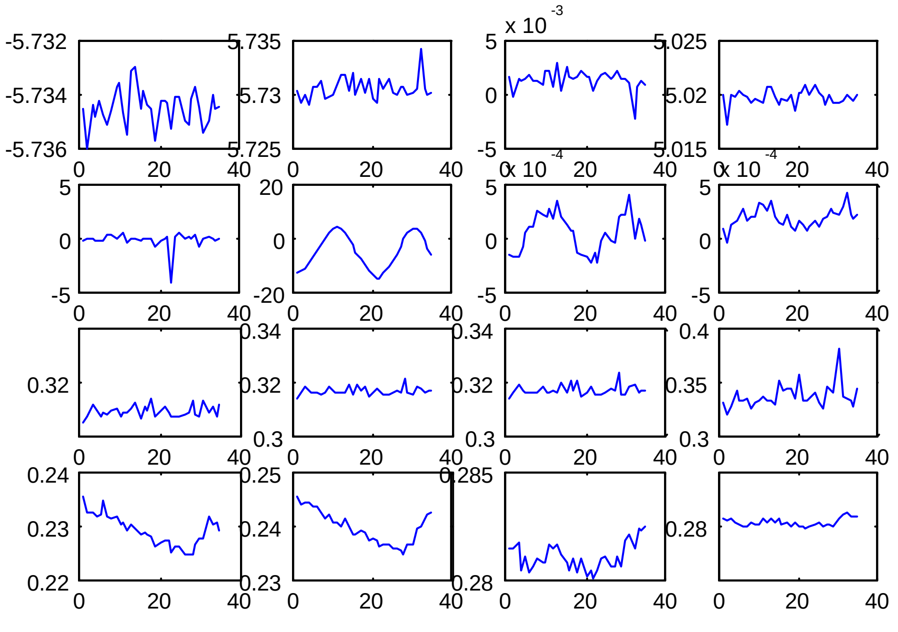

X axis hours Y axis = V

Fig.8

The first graph is an example of LVDT readout, the second is the DAQ computer screen with the monitor signals. The window from 1 to 4 are the voltage readout from a circuit, useful to monitor instantaneously the LVDT ality function or not. The window 5 is the duty cycle coming from the heater inside the oven that contains the totem. The window 6 is the duty cycle cooling fan inside the box that contains the electronics. The windows since 9 to 12 are thermometers inside the oven, The windows 13 and 14 are the external thermometer and the windows 15 and 16 are the thermometer inside the electronics box.

A similar program has been used to check possible cross talks between the digital controller signals and the LVDT readout channels, which were present in the past. This effect was shown to absent in the present setup. A variant of this program has been used to check the system temperature stability.

Chapter
5

Preliminary System Tests

- The signal shown in the LabView data acquisition graphs seemed present to some cross talks between the digital controller signals. In fact the signals seemed to step up and down in correspondence with the switch of the temperature controller.
  To check if there is a correlation between the switch signal and the LVDT signal, a special program reads the data from the test run and compares the signal coming from a LVDT with signal switch on or off.
  The LVDT signal is averaged both with switch on and off and the difference is made between each high and low .
  The program does a histogram on those differences. We obtain a zero centered histograms, ruling out that the switch channel influence the LVDT channels.

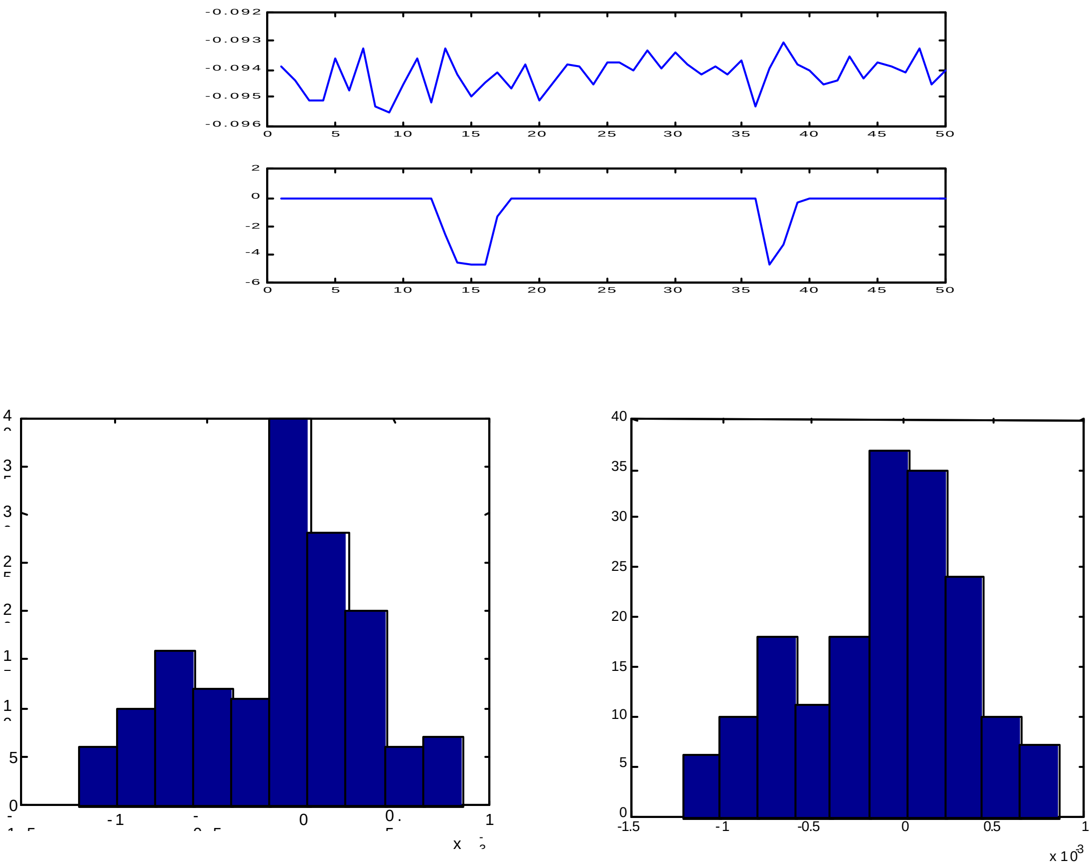

Fig.9.

- To check the stability LVDT drivers for different power supply voltage of the system, we acquired a LVDT signals changing the power supply voltage and the result is that there are not important effects on the signals.

- To test the temperature stability of LVDT drivers, we warmed the different electronic components checking the LVDT readout and found that some resistors and capacitors inside of LVDT drivers were not stable in temperature. We substituted those components and remade this test obtaining more stable electronics.

- To test the temperature and frequency stability of the Master Oscillator (see scheme in following page) we warmed it using a frequency signal from 12 KHz to 15 KHz . In fact , during the measurements we use it with a frequency signal of 14 KHz . The result is that there are not effects on the signal.

Chapter 6

LVDTs calibration

In the preliminary acquisition to test the system, we acquired data for many days uninterruptedly and the LVDT signal seemed to be affected by a drift due to some system instability.

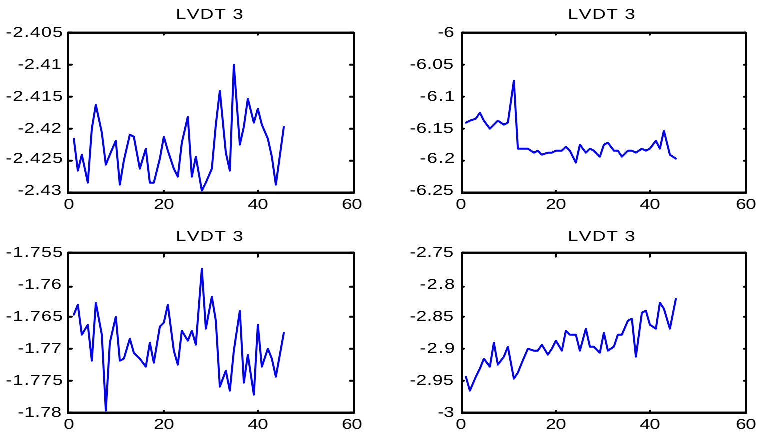

X axis = hours Y axis = V

Fig. 10. Stability plots from the analysis program.

We could see in the second graph the jump of about 30 mV and in the last one a drift of 10 mV.

For this reason we remade the LVDTs calibration. The characteristic LVDT calibration curve is shown in the following figure. The graph represents the LVDT readout voltage as a function of the primary coil movement. As it is shown, there is a zone in which the LVDT signal curve is proportional to the primary coil movement. The linear zone is the working range of LVDT.

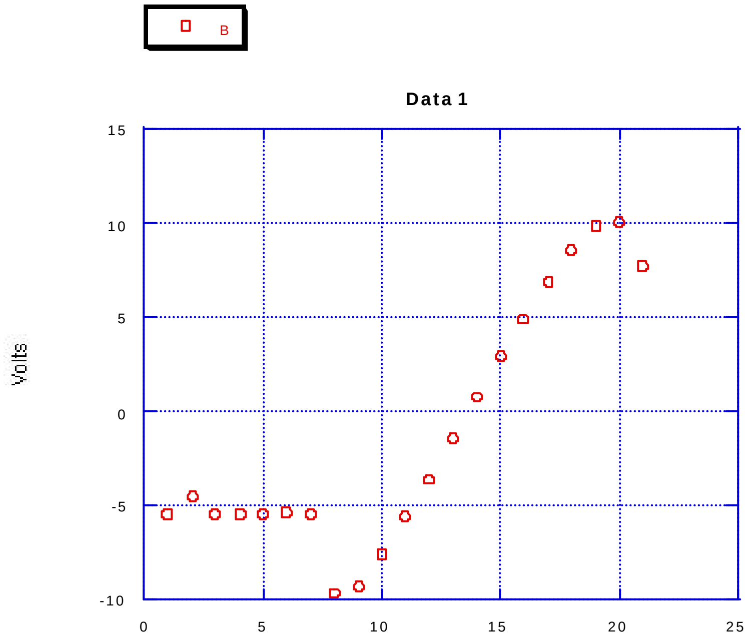

Fig. 11. LVDT calibration

Moreover it is possible to change the amplifier gain inside the LVDT drivers to regulate the slope. We chose a sensivity of 3.5 V / mm and mechanically regulated the primary coil of each LVDT in position corresponding to middle of the linear zone.

Chapter
7

Mechanics assembles

Finally we assembled the mechanics on the support structure called “totem”. We mounted different kinds of blades in thickness and length on the totem using a hydraulic bending system and then loaded the blades with different weights corresponding to the rated load, to bring the blade stip in horizontal position.

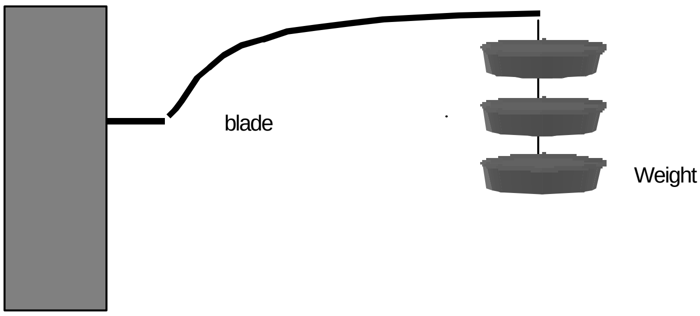

Fig. 12

Blade’s characteristics are shown in the following table of the eight blades used in the test.

Blade number	Loads (Kg)	Thickness (mm)	Length (cm)
8	115.49	4.0	20.8
7	115.66	4.0	20.8
0	71.04	4.0	29.2
6	48.66	3.0	20.8
5	48.56	3.0	20.8
2	34.54	3.0	29.2
9	76.2	4.0	29.2
4	51.06	3.5	29.2

We started the acquisition choosing to acquire at 250 Hz and write a data point every four second.
The oven temperature was 30°C.

Chapter
8

First results, problems to solve and following steps

In the first of acquisition, we discovered a strange blade's behavior.
The graphs of the position in detail showed a strange jumps.

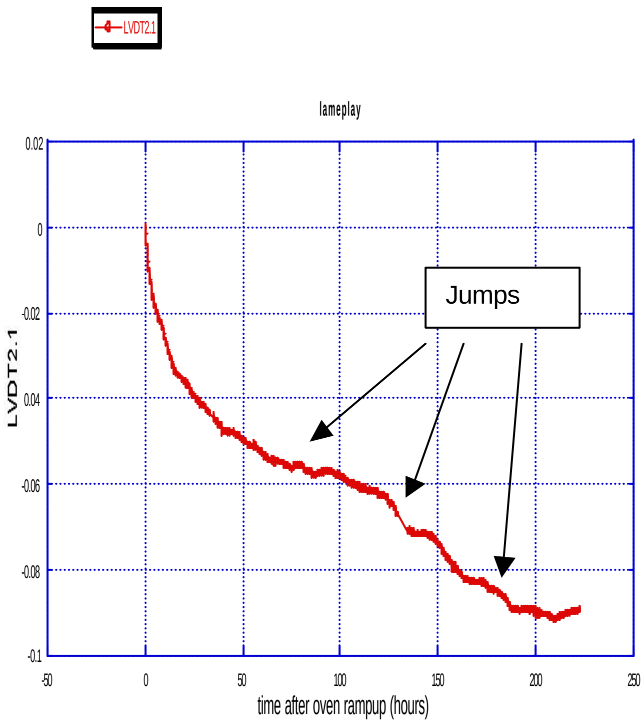

Steps were often happening in groups and during human activity, but in a seemingly random combination, some up, some down and some no visible effect.

For long time we suspected data acquisition problems with the assumption that no mechanical event will raise the position of the masses attached to the blades. If a catastrophic creep or slipping event must happen it will be only downward.

Finally on Sept. 26th at 18:49 we had a small earthquake.
The earthquake produced large LVDT reading changes, on some blades

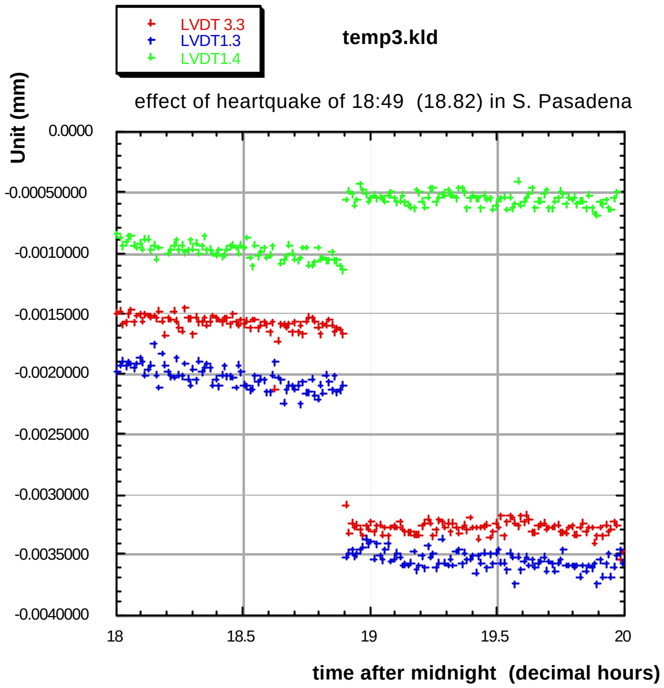

Small or no steps on other blades:

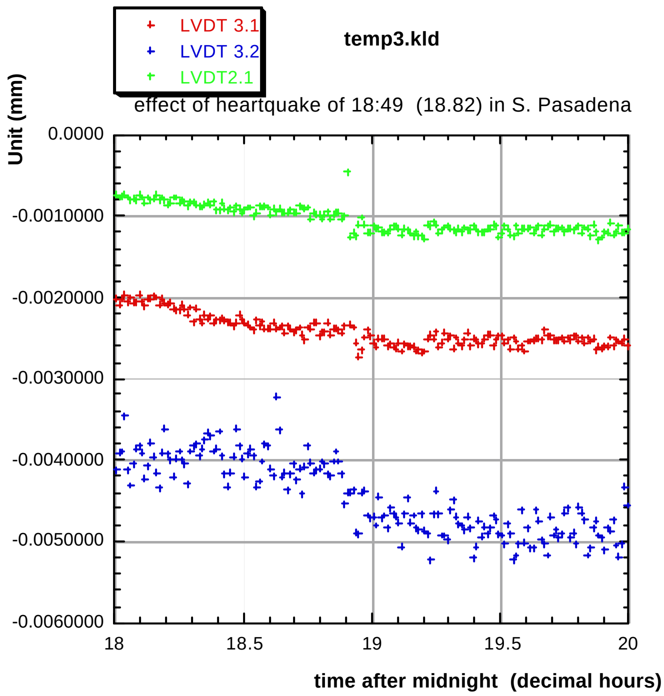

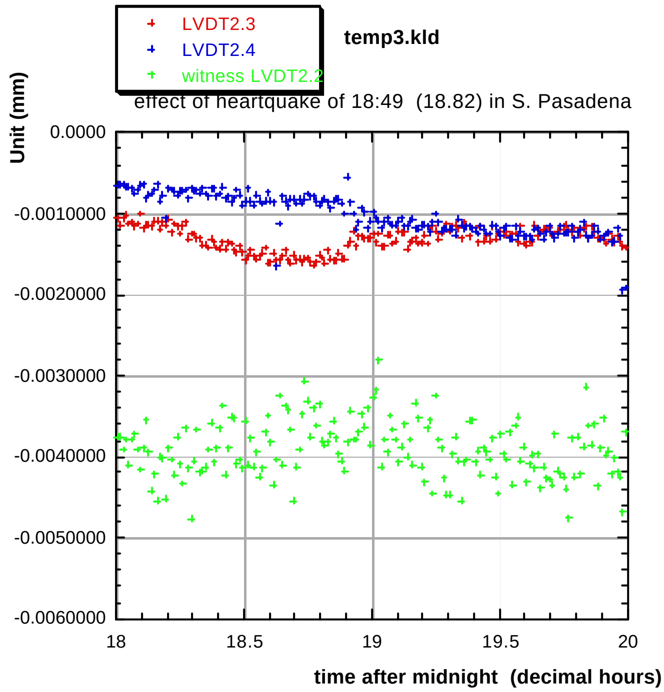

The only possible explanation being that the verticality of the center column of the totem was tilted on one side by, 100 to 200 microradians. If this tilt happens the blades on one side will raise while the blades on the other side will lower and the blades in front and back will not be (or be little) affected. Each blade will respond with a step proportional to the amplitude of the tilt in its longitudinal direction, times its integrated elongation from its at rest position to its loaded position. Of course no earthquake effect is visible on a witness LVDT.
This large events finally seems to explain some of the multiple small event visible during the Minos working time. The observed small steps can be easily explained with small (10 microradian) shift of verticality of the totem, which in their turn can be explained with the overhead crane movements.

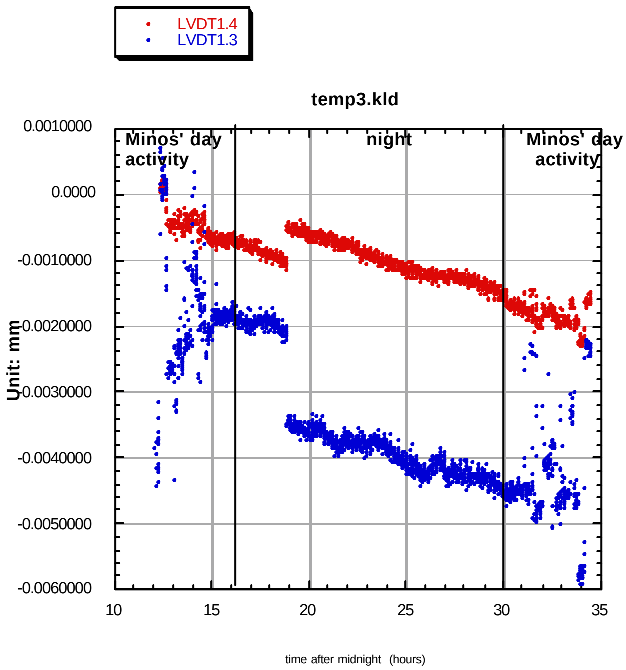

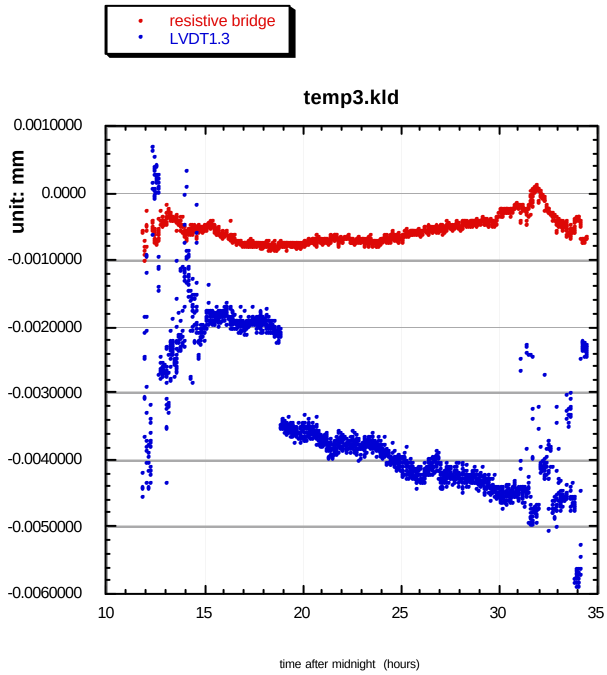

One could think of just gating out the daytime data and measure the creep with the remaining night time data. Occasional earthquake events could be reconnected by hand. The problem with the Minos activity is that at the end of the day it does not leave the totem in the original verticality and it is difficult to determine the integrated tilt and the creep measurement is strongly polluted.

One only solution seems to be to suspend the totem pole from its top with the aid of a wire.
Then the totem will hang down and supposedly find its verticality. Of course it will be useful to mount identical blades in opposite positions to both balance the totem pole and allow filtering of the differential mode of the residual variations of verticality.

If we switch the graphs suppressing the jumps the graphs look like the followings, witch correctly follow the logarithmic behavior

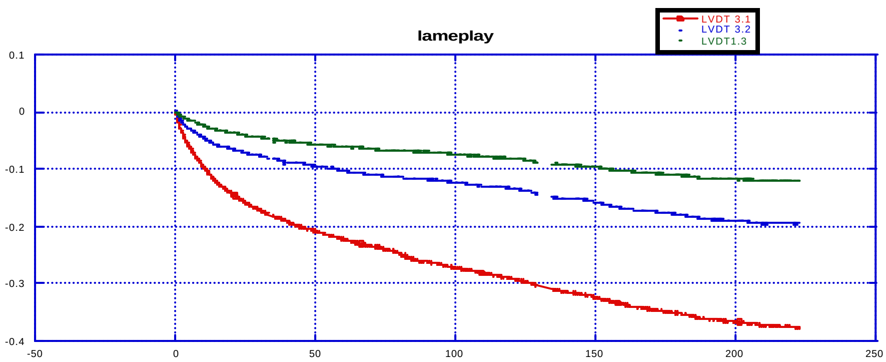

Fig 14.

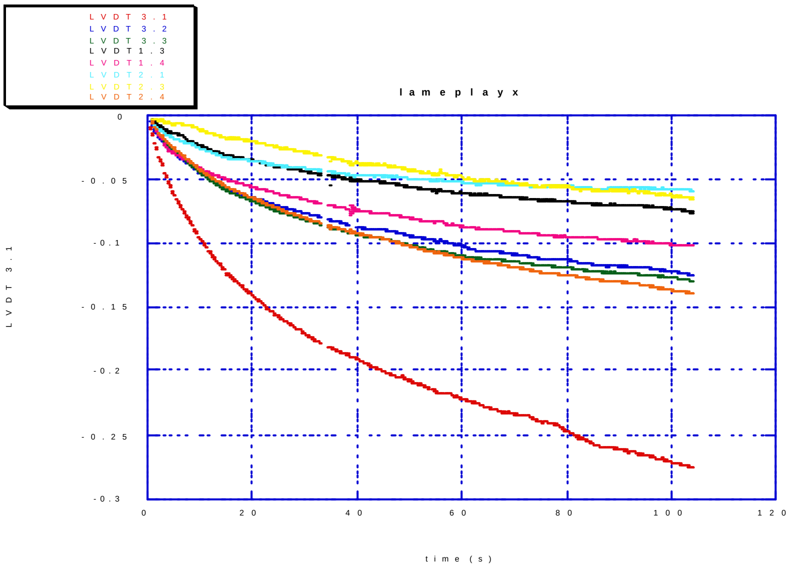

Fig 15.

Happily no linear behavior is visible at least not yet.
Although this data is not believable, the behavior of fig. 14 and 15 indicates that, once solved the observed problems, the system will be able to correctly measure creep.